GSA Data Repository 2017256

Łuszczak, K., et al., 2017, How local crustal thermal properties influence the amount of denudation derived from low-temperature thermochronometry: Geology, doi:10.1130/G39036.1.

Contents

Section DR-1

(a) Sample preparation

Every rock was crushed and sieved to <500 μm. The apatite crystals for the analyses were extracted from the host rock using standard density and magnetic separation methods (Gemini shaking table, vertical and horizontal Frantz magnetic separator, LST and DIM heavy liquids).

(b) Apatite fission track analysis

The analysis was performed using the external detector method (Hurford and Green, 1982). The apatite grains were mounted in an epoxy resin, polished and etched for 20 seconds in 5.5 Molar HNO_3 at constant temperature of 20 ± 1ºC and packed with low U-mica sheets and IRMM-540 standard glasses (dosimeter). The samples were irradiated with a low energy neutron flux at the Oregon State University Radiation Centre, USA. The irradiated mica sheets were etched for 20 minutes in concentrated HF.

The fission track analysis was carried out in the University of Glasgow fission track laboratory using a Zeiss Axioplan microscope (magnification: x1250) with a Trevor Dumitru stage system and the FT Stage 4.04 software. Only isolated apatite grains, with a polished surface parallel to the crystal c-axis, free of cleavage and large fractures, with a minimum countable area of 2200 μm^2 (preferably >6000 μm^2) were counted. When applicable, at least 20 grains were analyzed. At least 5 diameters of the fission track etch pits (D-Par) were measured per grain, as a proxy to take the apatite chemical composition into account (Donelick et al., 1999) (Table DR-2). The apatite fission track single grain ages, central and pooled ages and χ^2 test were calculated using TrackKey software (Dunkl, 2002).

The lengths of horizontal, confined fission tracks were measured on the grains parallel to the c-axis along with a determination of at least five D-Pars and the angle of the track with the c-axis. When possible, at least 100 tracks were measured per sample. Wherever possible, only TINT tracks (track- in-track) were measured.

Section DR-2

(a) Quantifying thermal histories (QTQt)

Apatite fission track data were modeled using the QTQt software (Gallagher, 2012) to extract thermal histories. The general prior time-temperature box was set at temperature of 75 ± 75ºC and the range set for time was based on the oldest observed age (the oldest age ± the oldest age). Most of the samples come from intrusive rocks, for which the only available thermal constraint is the age of emplacement. All the granitic intrusions in southern Scotland and Lake District belong to the 'Newer Granites' suite and yield biotite K-Ar ages ranging from 390 to 440 Ma (Brown et al., 1964, 1968, Halliday et al., 1979, Rundle, 1979). The initial time-temperature constraints applied for the models have been set to 300 ± 100ºC at 400 ± 20 Ma. The Crawfordjohn essexite from the northern most part of the Southern Uplands is a Variscan dyke, emplaced in the Late Carboniferous–Early Permian (Stephenson, 2003); the initial constraints box was set to 300 ± 20 Ma and 300 ± 100ºC.

In the case of sedimentary samples, the stratigraphic age was used as an additional constraint. For the granite boulder from the Ordovician conglomerate at Corsewall Point two constraints have been used: the emplacement age of the granite, 474 ± 15 Ma and 300 ± 100ºC and the depositional age 458 ± 2 Ma and 20 ± 20ºC based on the ages determined by Bluck et al., (2006). The timing of the intrusion and cooling of granites in north Wales is not well constrained; for the Llŷn intrusions that are early Caledonian (Ordovician) (Croudace, 1982) the initial constraints of 460 ± 20 Ma and 300 ± 100ºC were used.

Samples were modeled individually. Only three samples from Fleet granite were modeled together, as they were collected from less than 5 kilometres from each other; the higher number of data gives stronger constraints on the modeling results.

All models were run for at least 200 000 iterations ('post-burn-in') after discarding initial 50,000 iterations ('burn-in'). For the fission track annealing kinetics, the multi-kinetic annealing model of Ketcham et al., (2007) was chosen. Compositionally dependent initial

track lengths were calculated based on an input D-Par value for each grain, calibrated against Durango standard.

Thermal histories and model predictions are given in Fig. DR-1. The Late Cretaceous temperatures for all samples are given in Table DR-2. Paleotemperatures were read from the obtained time-temperature paths for the modeled samples for which both the age and the fission track length distribution are available. In the case of samples without track lengths data, paleotemperatures were estimated based on the given age and the thermal histories of rocks in the surrounding area.

(b) 1-D heat transfer modeling (Exhume)

The Exhume code used in 1-D modeling of heat transfer was provided by Prof. Kerry Gallagher, who is kindly thanked. The code solves the heat transfer equation in one dimension (vertical) within a layered crust or lithosphere, under a steady-state or experiencing one or several episodes of erosion.

All models assume a constant basal heat flow of 30 mW/m^2, a constant surface temperature of 10°C and a 100 km thick lithosphere, including a 70 km thick lithospheric mantle (H = 0 $\mu W/m^3$, k = 2.5 W/m/K) and a 30 km thick crust with variable thermal properties (in the 'normal' crust, without the heat-generating granite and the sedimentary blanket: H = 1 $\mu W/m^3$, k = 2.5 W/m/K). The geotherms are calculated for a lithosphere in steady state.

(c) 3-D heat transfer modeling (Pecube)

Pecube is a finite element model solving the 3-D version of the heat equation (Braun et al, 2012). It predicts low temperature thermochronological ages for an input tectonic scenario and changes of the topography. The recent version of the model allows to modify spatial variability of the heat production rate (A) and thermal diffusivity (K) values.

In all scenarios the model thickness was set to 30 km, with the basal and surface temperatures of 550°C and 10°C, respectively. The uplift function is spatially uniform with

rapid uplift between 62 and 57 Ma and slow uplift thereafter. The rate of uplift is tuned to produce a set amount of total uplift; for example, to obtain a total uplift of 2.25 km, the rapid uplift rate was set to 0.33 km/Myr and slow uplift rate to 0.0088 km/Myr. At the beginning of every scenario there is no topography; we assume that the present-day topography (derived from 1 arc–minute ETOPO1 "Bedrock" Digital Elevation Model) is progressively created between 60–0 Ma. In order to shorten computing time, skipping factor for the DEM resolution was set to 10. Pecube deals with topography changes and rock uplift separately; the exhumation is calculated after Molnar and England (1990), as a difference between the regional rock uplift and changes in elevation of the surface.

In the uniform crust scenario (UC), thermal parameters A and K were spatially constant. In scenario G0, 12 km thick cylinder with radius (r) of 36 km was placed in the Lake District and three smaller cylinders (r = 10 km, thickness = 12 km, each) in south Scotland to mimic Criffell, Fleet and Loch Doon granites. The same geometry was then used in scenario GS, where the whole area was additionally covered by 1–2 km thick layer of low thermal diffusivity.

The values of the heat production measured in the intrusive rocks in central west Britain and the thermal conductivity measured in the Mesozoic sedimentary rocks preserved elsewhere in Britain are given in Tables DR-3 and DR-4, respectively. In Pecube, these parameters have to be input as heat production rate ($A = H/ \rho /c$, where H is heat production, ρ is density, and c is specific heat capacity) and thermal diffusivity ($\kappa = k/\rho/c$, where k is thermal conductivity, ρ is density, and c is specific heat capacity). We used two values of thermal diffusivity: 15 and 10 km^2/Myr; 15 km^2/Myr is the measured average value for mudstone and chalk after Eppelbaum et al. (2014) and 10 km^2/Myr is a hypothetical value that would characterize less compacted sediments. For heat production we used two values for the Lake District batholith: 40 and 50ºC/Myr (for H = 3.2 or 4 $\mu W/m^3$) and two values for the batholiths is south Scotland: 25 and 30ºC/Myr (for H = 2 or 2.4 4 $\mu W/m^3$), calculated

assuming ρ = 2.63 kg/m^3 and c = 0.95 J/kg/K.

The models were evaluated based on the misfit (μ) between the measured (observed) and predicted AFT ages given by:

$$\boldsymbol{\mu = \frac{1}{N-p-1} \sum_{i=1}^{N} \frac{(O_i - P_i)^2}{\sigma_i^2}} \quad (2)$$

where N is the number of data points, p is the number of model parameters, O is the observed age, P is the predicted age and σ is the uncertainty of the observed age. Thermal parameters, amounts of total uplift and misfit values tested in the models are listed in Table DR-3.

(d) Limitations of 3-D heat transfer modeling

Several simplifications used in the modeling undoubtedly have an influence on the predicted ages. These include a simplified spatial distribution of thermal parameters and a lack of pre-Cenozoic uplift/subsidence events spatially uniform amount of uplift.

Heat producing granite batholiths were modelled as cylinders with homogeneous distribution of radiogenic elements. For the given amounts of uplift, the AFT ages in the heat producing areas are insensitive to changes in the heat production values. The assumption of vertically uniform heat production with depth also seems to be a good approximation for the Lake District batholith; if the concentration of the radiogenic elements decreases exponentially with depth (a commonly occurring phenomenon in granitic intrusions), for the given values of heat production in the sub-surface rocks, the observed surface heat flow would be underestimated. The shape of the heat productive bodies definitely has an influence on the predicted pattern of the ages. However, for the given data set, small misalignment of the batholiths edges would not make significant changes to the misfit, as the sampling locations are far away from the batholith edges.

The model assumes constant thickness of the sedimentary layer that covers the whole region uniformly. Certainly, the coastal areas have experienced higher sedimentation and the highs had thinner cover, if any. The AFT ages in the Lake District are, however, insensitive to

the amount of sediments, if the uplift was higher than 3 km. The use of a variable thickness of the sedimentary layer would require the thermal conductivity value to vary with depth, however, in the case of a 'thin' 1.0-1.5 km thick blanket, such changes will not be significant.

The model assumes that the uplift was spatially uniform. There is no direct indication that this assumption is wrong, as some of the most probable uplift mechanisms, such as the mantle plume-derived thermal anomaly, cause a spatially uniform uplift. The underplating material is, however, thicker in western Britain, implying a differential uplift, decreasing eastward (Al-Kindi et al., 2003). Local-scale differences in the amount of uplift may explain ages that cannot be fully predicted by the models.

The use of a simple uplift scenario, with no tectonic events prior to the Cenozoic may have a non-negligible influence on the derived ages. The geological constraints clearly indicate that this simple scenario is not accurate and that the pre-60 Ma history of central west Britain was complex. However, the main aim of the 3-D modelling is to explore the influence of the crustal thermal heterogeneities on the AFT ages. Investigating the pre-Cenozoic geological history of the area is beyond the scope of this modelling experiment. The AFT ages in the Lake District indicate that rocks now at the surface were at temperatures higher than the Partial Annealing Zone in the pre-Cenozoic and, therefore, their previous history has no effect on the available thermochronometric data. Admittedly, the pre-60 Ma history has an influence on the AFT ages in south Scotland and north Wales; in these cases, the amount of Cenozoic uplift estimated by the models should be considered as a maximum. The effect of the presence of heat producing rocks and of a blanketing sedimentary cover is still valid.

Figure DR-1: Thermal histories and model predictions extracted from inverse modeling using the QTQt software (Gallagher, 2012). Thermal history graphs: thick red line is the maximum likelihood model; thick blue line is the expected model and dashed blue lines are the 95% credible intervals; thin red line defining a box shows the general range of prior; the light yellow shadow marks the Cenozoic era, 66–0 Ma. Although most of the models start from temperatures of 300 ± 100°C (see text for more details), as the AFT data do not provide constraints at such high temperatures, the temperature space shown on the graphs is 0–150°C. Model predictions graphs present predictions for projected fission track length distribution (FTLD); the histogram shows the observed data, the red and gray lines are the predicted FTLD and the 95% credible intervals, respectively; the numbers in the top left corner are the observed (O) and predicted (P) AFT age, MTL and D-Par.

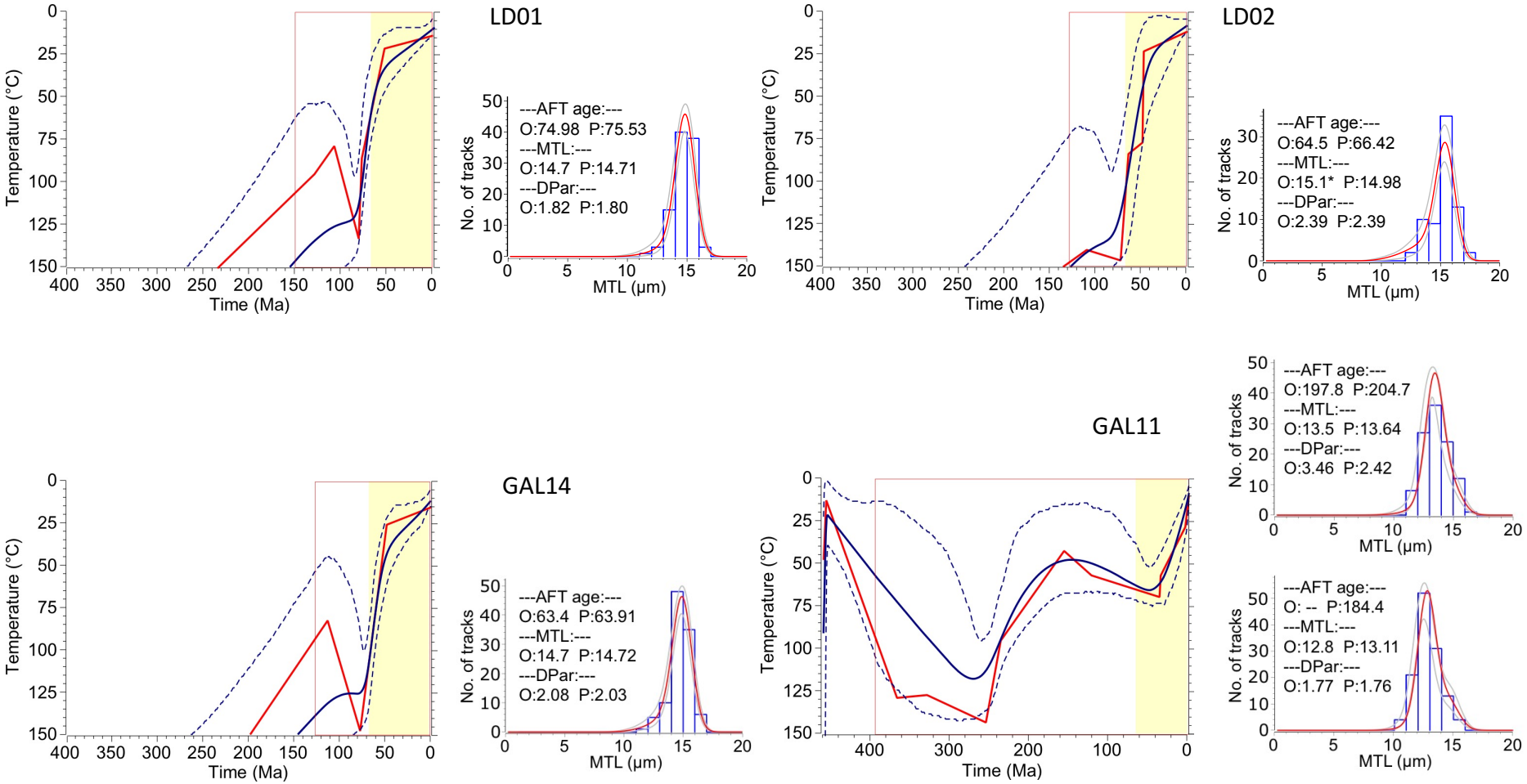

Figure DR-1: (continued)

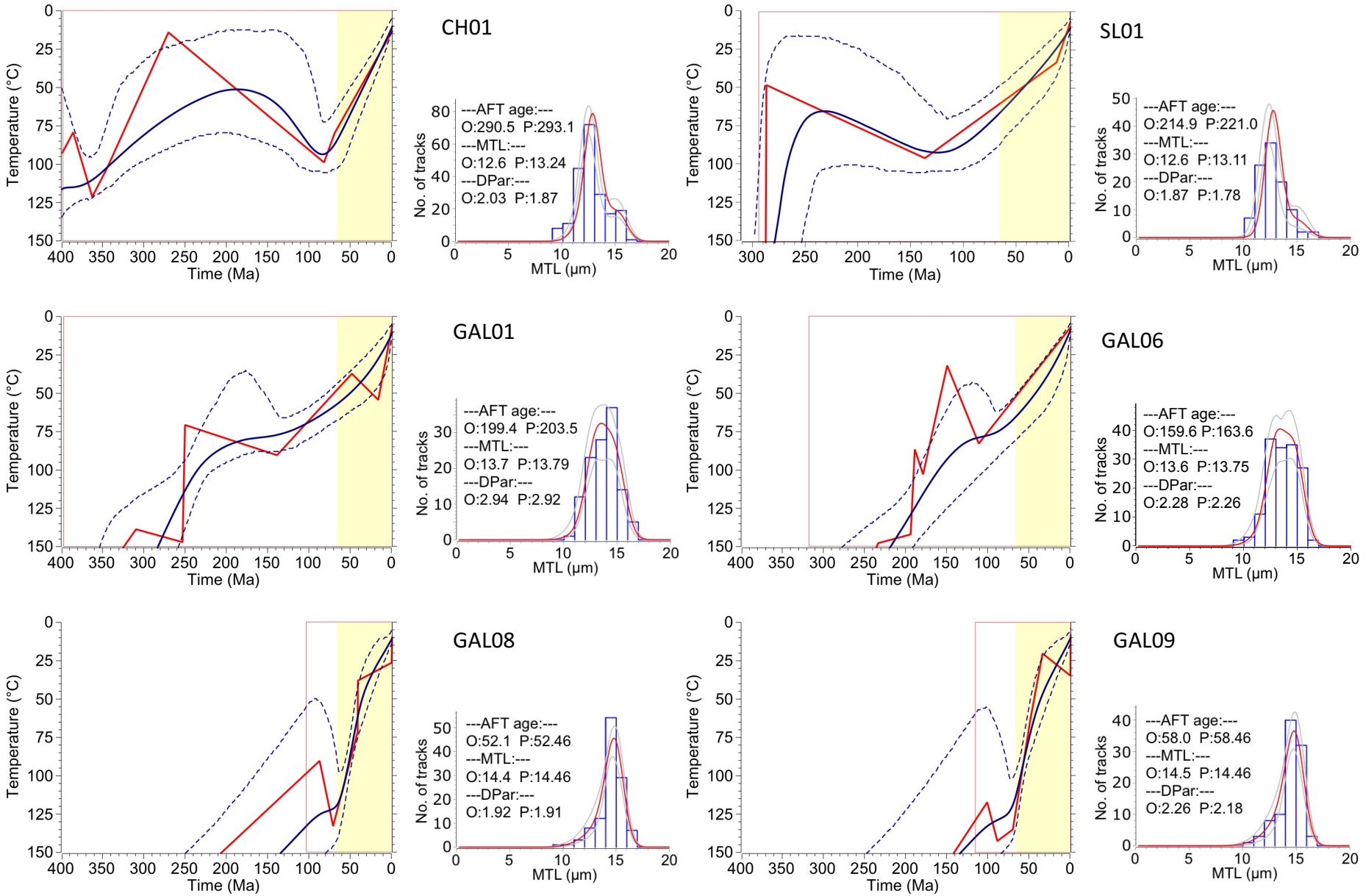

Figure DR-1: (continued)

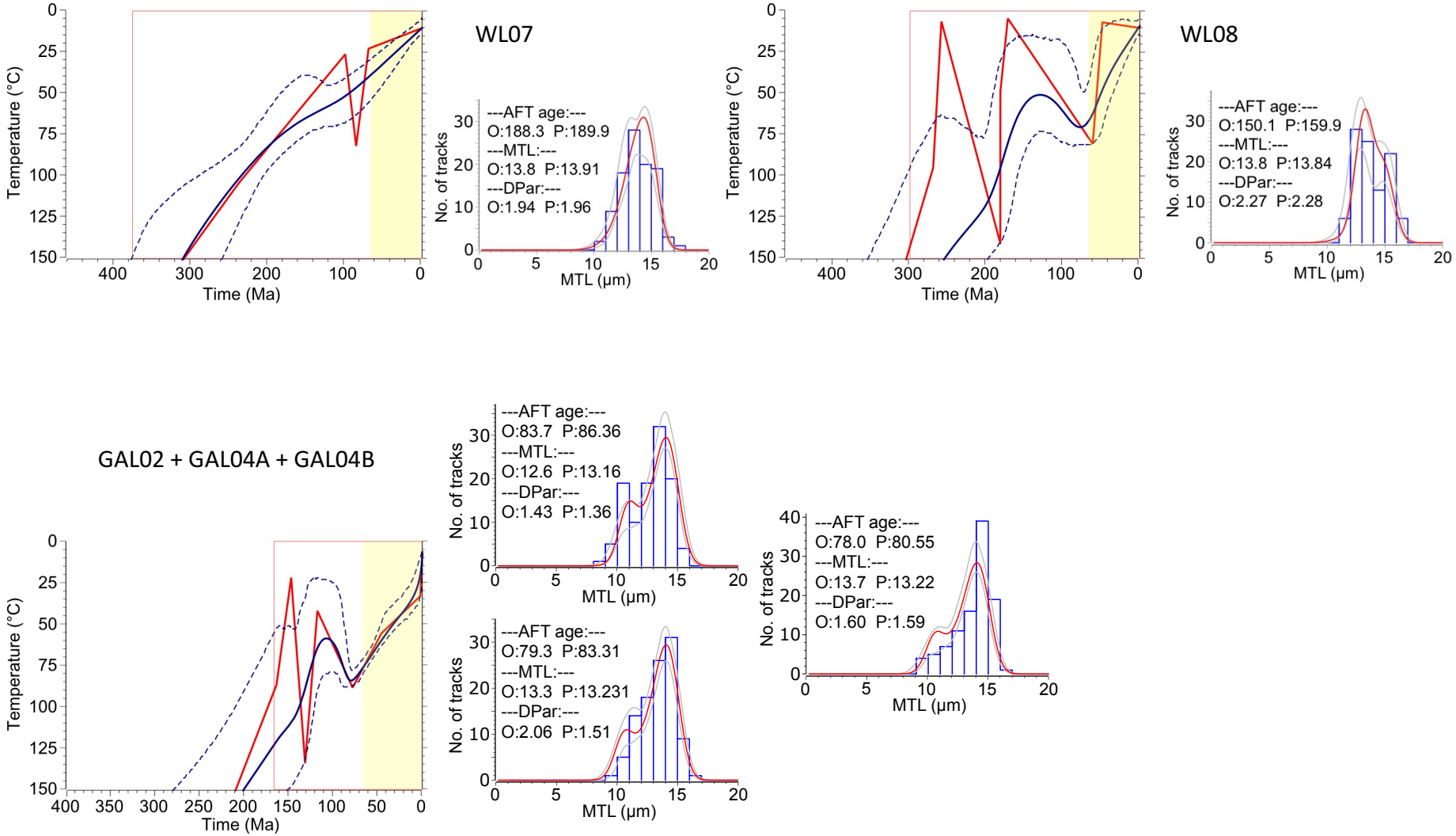

Figure DR-2: Impact of emplacement of magmatic underplating on geotherms in the lithosphere. The graphs (1-D) show the geotherms at 61, 59, 57 and 55 Ma for different thicknesses of a magmatic underplating that was emplaced instantaneously at 62 Ma in the lowest part of the crust (between 20-29 km and 30 km); the initial temperature of the magma is 1100°C. Left panel – temperature changes within the lithosphere up to a depth of 50 km; right panel – temperature changes within the uppermost 4 km of the crust. Note almost no change of temperature in the uppermost crust for underplating thickness <5 km (observed values in onshore central west Britain; Al-Kindi et al., 2003), and only a little change for thickness of 10 km. Note also a fast shrinking of the thermal anomaly.

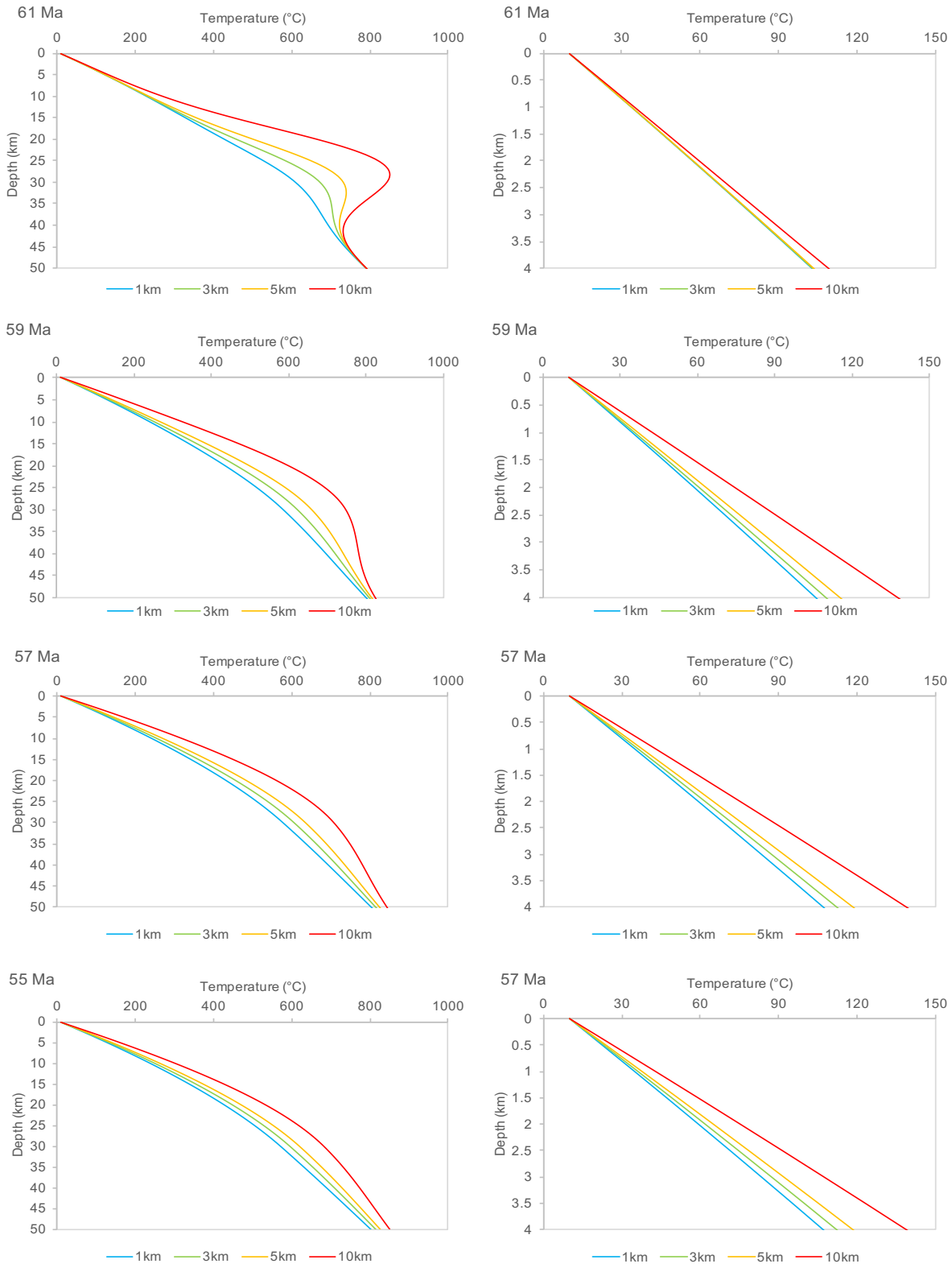

Table DR-1: Sample location and rock details.

Sample name	Lat (°N)	Long (°W)	Elevation (m)	Intrusion/location name*	Lithology	Emplacement/depositional age†
Lake District						
LD01	54.4690	2.6881	380	Shap	granite	Early Devonian
LD02	54.6911	3.0098	445	Carrock	gabbro	Late Silurian/Early Devonian
LD05	54.6102	3.0408	192	Threlkeld	microgranite	Late Silurian
LD10	54.6410	3.0911	347	Skiddaw	granite	Early Devonian
LD12	54.5297	2.7825	258	Haweswater	gabbro	Early Devonian
LD18	54.5456	3.5980	10	*Whitehaven*	sandstone	*Late Carboniferous*
South Scotland						
GAL01	55.2174	4.3966	224	Loch Doon	granodiorite	Early Devonian
GAL02	55.0434	4.1212	50	Fleet	granite	Early Devonian
GAL04A	55.0358	4.2145	110	Fleet	granite	Early Devonian
GAL04B	55.0358	4.2145	110	Fleet	granite	Early Devonian
GAL06	54.6773	4.9650	50	Portencorkie	diorite	Early Devonian
GAL08	54.9297	3.8132	56	Criffell	granodiorite	Early Devonian
GAL09	54.9240	3.8057	60	Criffell	granite	Early Devonian
GAL11	55.0076	5.1592	1	*Corsewall Point*	conglomerate (granite boulder)	*Ordovician*
GAL14	54.9380	3.7949	65	Criffell	granite	Early Devonian
SL01	55.4956	3.7126	310	Crawfordjohn	essexite	Late Carboniferous/Early Permian
CH01	55.4872	2.0916	260	Cheviot	granite	Early Devonian
North Wales						
WL02	52.9037	3.2040	168	*Glyn Ceiriog*	diorite	Ordovician
WL05	52.9862	4.4362	219	Granfor	tonalite	Ordovician
WL06	52.9862	4.4362	220	Granfor	tonalite	Ordovician
WL07	52.9498	4.5045	26	Penrhyn Bodeilas	tonalite	Ordovician
WL08	53.2624	3.9270	200	*Penmaenmawr*	granophyre	Ordovician

*Intrusion names are given for intrusive rocks, when available. Location names are given in italics for no named intrusions and sedimentary samples.
†Emplacement ages are given for all plutonic rocks. Depositional ages are given in italics for sedimentary rocks. See Section DR-2a for references.

Table DR-2: Apatite fission track data and paleotemperature estimates for each sample. Paleotemperatures are derived from modeling of apatite fission track data using the QTQt software (Gallagher, 2012). ρ_D – fission track density on dosimeter, ρ_s – spontaneous fission track density, ρ_i – induced fission track density, N_D – number of fission track on dosimeter, N_s – number of spontaneous fission tracks, N_i – number of induced fission tracks, P – probability, MTL_m – mean track length (measured), MTL_p – mean track length (projected).

Sample name	ρ_D (cm^2)	ρ_s (cm^2)	ρ_i (cm^2)	X^2	age ± 1σ (Ma)	MTL_m ± 1σ (μm)	MTL_p ± 1σ (μm)	DPar ± 1σ (μm)	Late Cretaceous paleotemperature (°C)
No. grains [lengths]	N_D	N_s	N_i	P (%)					
Lake District									
LD01	1.27E+06	6.33E-07	1.67E-06	16.5	75.0 ± 3.1	13.14 ± 1.78	14.35 ± 1.29	1.82 ± 0.08	120 ± 20
22 [110]	8874	1608	4247	73.9					
LD02	1.23E+06	7.06E-08	2.10E-07	9.2	64.5 ± 6.2	13.79 ± 1.36	14.90 ± 0.97	2.40 ± 0.11	120 ± 20
20 [16]	8874	157	467	96.9					
LD02_len*	-	-	-	-	-	14.55 ± 1.49	15.39 ± 0.99	2.99 ± 0.52	-
0 [76]	-	-	-	-	-				
LD05	8.87E+05	4.52E-07	8.17E-07	3.1	74.9 ± 7.6	-	-	-	120 ± 30†
11 [0]	6478	164	303	98					
LD10	8.83E+05	4.47E-07	1.11E-06	14.6	55.4 ± 3.6	14.16 ± 1.14	14.87 ± 0.83	2.20 ± 0.13	120 ± 30†
17 [10]	6478	435	1083	48.3					
LD12	8.87E+05	1.09E-07	3.83E-07	4.2	35.9 ± 8.5	-	-	-	120 ± 30†
7 [0]	6478	23	89	65.2					
LD18	8.71E+05	5.77E-07	1.61E-06	18.5	48.5 ± 3.1	-	-	3.78 ± 0.42	120 ± 20†
16 [0]	6478	459	1285	23.9					
South Scotland									
GAL01	9.44E+05	2.48E-06	1.83E-06	30.5	199.5 ± 8.9	12.67 ± 1.75	13.73 ± 1.32	2.94 ± 0.14	60 ± 15
20 [120]	6478	3217	2353	4.6					
GAL02	1.24E+06	5.79E-07	1.38E-06	19	78.1 ± 4.4	12.69 ± 2.31	14.14 ± 1.28	1.57 ± 0.11	85 ± 10
19 [102]	8874	620	1537	39.1					
GAL04A	9.36E+05	1.44E-06	2.45E-06	9.3	83.7 ± 3.8	13.76 ± 1.83	14.61 ± 1.48	1.47 ± 0.18	85 ± 10
18 [76]	6478	1346	2346	93.2					
GAL04A_len*	-	-	-	-	-	11.21 ± 2.30	13.17 ± 1.35	1.43 ± 0.10	-
0 [110]	-	-	-						

GAL04B	9.31E+05	1.13E-06	2.11E-06	36.5	79.3 ± 4.5	12.37 ± 1.87	13.4 ± 1.32	2.24 ± 0.12	85 ± 10
20 [105]	6478	1302	2315	0.9					
GAL06	9.27E+05	1.22E-06	1.11E-06	23.9	159. ± 7.3	13.32 ± 1.79	14.51 ± 1.18	4.64 ± 0.72	70 ± 10
20 [99]	6478	1959	1760	19.9					
GAL06_len*	-	-	-	-	-	12.46 ± 1.87	14.00 ± 1.21	2.28 ± 0.09	-
0 [151]	-	-	-						
GAL08	1.22E+06	4.58E-07	1.66E-06	22.8	52.1 ± 2.5	13.59 ± 1.59	14.7 ± 1.07	1.92 ± 0.08	120 ± 20
20 [115]	8874	988	3615	24.8					
GAL09	1.21E+06	6.43E-07	2.12E-06	25.8	58.0 ± 2.9	13.74 ± 1.50	14.78 ± 1.01	2.26 ± 0.21	120 ± 20
21 [97]	8874	993	3226	17.2					
GAL14	1.22E+06	6.07E-07	1.84E-06	16.5	63.4 ± 2.8	13.89 ± 1.33	14.94 ± 0.87	2.07 ± 0.12	120 ± 20
24 [105]	8874	1148	3450	83.2					
GAL11	9.23E+05	1.43E-06	1.04E-06	46	197.9 ± 10.1	12.43 ± 1.54	13.89 ± 1.00	3.46 ± 0.90	65 ± 10
20 [108]	6478	3167	2272	0.1					
GAL11_len*	-	-	-	-	-	11.34 ± 1.53	12.83 ± 1.01	1.77 ± 0.09	-
0 [125]	-	-	-						
SL01	1.25E+06	4.65E-07	4.10E-07	8.4	215.0 ± 14.3	11.20 ± 1.72	13.14 ± 1.09	1.82 ± 0.08	65 ± 15
24 [101]	8874	582	522	99.8					
CH01	1.20E+06	4.32E-06	2.80E-06	53.6	290.5 ± 13.2	11.08 ± 2.04	13.14 ± 1.21	2.04 ± 0.16	90 ± 15
20 [202]	8874	5289	3339	0					
North Wales									
WL02	9.11E+05	1.16E-07	9.43E-08	4.4	172.1 ± 28.6	-	-	-	50 ± 30†
19 [0]	6478	83	68	100					
WL05	1.26E+06	5.62E-07	5.82E-07	11.1	187.0 ± 13.7	-	-	1.61 ± 0.11	60 ± 20†
21 [0]	8874	431	449	94.4					
WL06	9.03E+05	5.22E-07	3.75E-07	32.3	195.5 ± 20.1	-	-	1.86 ± 0.09	60 ± 20†
20 [0]	6478	422	295	2.9					
WL07	8.99E+05	3.38E-07	2.44E-07	4.4	188.4 ± 14.2	12.89 ± 1.74	13.82 ± 1.41	1.94 ± 0.15	60 ± 20
19 [100]	6478	488	360	100					
WL08	8.95E+05	4.22E-07	3.87E-07	13.4	150.2 ± 11.2	12.82 ± 1.81	13.81 ± 1.36	2.26 ± 0.07	70 ± 15
20 [100]	6478	447	413	81.9					

The apatite fission track ages were calculated using a Zeta value of 312.7 ± 8.3.

*The second slide was prepared for fission track lengths determination only, to increase the number of data available.

†Not modeled due to the lack of track lengths measurements, estimated based on the age and thermal histories of rocks in the surrounding area.

Table DR-3: Heat production measured in the granite intrusions in central west Britain, after Downing and Gray (1986) and references therein.

Intrusion name	Heat production ($\mu W/m^3$)
Shap	4.3 (5.2)*
Skiddaw	3.5 (4.2)*
Ennerdale	2.8
Eskdale	1.9
Threlkeld	1.9
Weardale	3.7 (4.1)**
Loch Doon	2.5
Fleet	3.0
Criffell	2.2
Cheviot	3.0

*value in brackets refers to heat production estimated from borehole and surface data (Downing and Gray, 1986, Lee et al., 1987)
**value in brackets refers to the average heat production measured in granite from the Eastgate borehole (Manning et al., 2007)

Table DR-4: Thermal conductivity of the most common Mesozoic lithostratigraphic formations in Britain, compiled after Downing and Gray (1986); Smst – sandy mudstone, Mdst – mudstone, Lmst – limestone, Sdst – sandstone, Slst: siltstone, Slcl – silty clay, Slmd – silty mudstone.

Formation	Lithology	Thermal conductivity (W/m/K)	Uncertainty
Cretaceous			
Chalk	Chlk	1.79	0.54
Upper Greensand	Sdst	2.66	0.19
Gault	Smst	2.32	0.04
	Mdst	1.67	0.11
Hastings Beds	Slst	2.01	
	Slcl	1.26	
Jurassic			
Kimmeride Clay	Mdst	1.51	0.09
Ampthill Clay	Mdst	1.51	0.03
Oxford Clay	Mdst	1.56	0.09
Kellaways Beds	Mdst	1.52	0.03
Cornbrash	Lmst	2.29	0.17
Forest Marble	Mdst + Lmst	1.80	0.07
Frome Clay	Mdst	1.72	1.10
Fullers Earth	Mdst	1.95	0.05
Upper Lias	Sdst	2.87	0.12
	Mdst	1.27	0.03
	Slmd	2.22	1.10
Middle Lias	Mdst	1.66	0.15
Lower Lias	Mdst	1.80	1.10
Triassic			
Mercia Mudstone Group	Mdst	1.88	0.03
	Mdst	2.28	0.33
Sherwood Sandstone Group	Sdst	3.41	0.09
	Mdst	2.37	0.23

Table DR-5: Parameters used in Pecube modeling and misfit values for particular models. A_0 – heat production rate in a uniform/background crust, κ_0 – thermal diffusivity of a uniform/background crust, A_{LD} – heat production in the Lake District batholith, A_{Scot} – heat production in small granite batholiths in south Scotland, κ_{sed} - thermal diffusivity of a sedimentary blanket, z_{sed} – thickness of a sedimentary blanket.

Model name	A_0 (°C/Myr)	κ_0 (km^2/Myr)	A_{LD} (°C/Myr)	A_{Scot} (°C/Myr)	κ_{sed} (km^2/Myr)	z_{sed} (km)	Uplift (km)	misfit
Uniform crust								
UC-01	12	25	-	-	-	-	4.00	10.8
UC-02	12	25	-	-	-	-	3.00	333.2
UC-03	12	25	-	-	-	-	3.50	141.8
UC-04	12	25	-	-	-	-	2.50	433.6
UC-05	12	25	-	-	-	-	4.50	7.6
UC-06	10	25	-	-	-	-	4.00	29.4
UC-07	10	25	-	-	-	-	3.00	367.7
UC-08	10	25	-	-	-	-	3.50	204.1
UC-09	10	25	-	-	-	-	2.50	450.0
UC-10	10	25	-	-	-	-	4.50	7.2
UC-11	15	25	-	-	-	-	4.00	7.1
UC-12	15	25	-	-	-	-	3.00	265.7
UC-13	15	25	-	-	-	-	3.50	54.4
UC-14	15	25	-	-	-	-	2.50	407.6
UC-15	15	25	-	-	-	-	4.50	8.0
Granite batholiths, constant thermal diffusivity								
G0-01	12	25	50	30	-	-	4.00	5.0
G0-02	12	25	50	30	-	-	3.00	142.6
G0-03	12	25	50	30	-	-	3.50	11.5
G0-04	12	25	50	30	-	-	2.50	319.4
G0-05	12	25	50	30	-	-	4.50	7.7
G0-06	12	25	40	25	-	-	4.00	5.0
G0-07	12	25	40	25	-	-	3.00	178.4
G0-08	12	25	40	25	-	-	3.50	24.4
G0-09	12	25	40	25	-	-	2.50	361.4
G0-10	12	25	40	25	-	-	4.50	7.7
G0-11	15	25	50	30	-	-	4.00	6.8
G0-12	15	25	50	30	-	-	3.00	101.2
G0-13	15	25	50	30	-	-	3.50	4.2
G0-14	15	25	50	30	-	-	2.50	291.3
G0-15	15	25	50	30	-	-	4.50	8.1
Granite batholiths and sedimentary blanket								
GS-01	12	25	50	30	10	1.0	4.00	8.1
GS-02	12	25	50	30	10	1.0	3.00	7.3
GS-03	12	25	50	30	10	1.0	3.50	8.0
GS-04	12	25	50	30	10	1.0	2.50	3.7
GS-05	12	25	50	30	10	1.0	2.00	25.5
GS-06	12	25	50	30	10	1.0	2.25	3.8
GS-07	12	25	50	30	15	1.0	4.00	7.8

GS-08	12	25	50	30	15	1.0	3.00	4.2
GS-09	12	25	50	30	15	1.0	2.50	103.9
GS-10	12	25	50	30	15	1.0	2.00	265.4
GS-11	12	25	50	30	15	1.0	2.25	176.6
GS-12	12	25	50	30	15	1.5	4.00	8.0
GS-13	12	25	50	30	15	1.5	3.00	3.5
GS-14	12	25	50	30	15	1.5	2.50	40.1
GS-15	12	25	50	30	15	1.5	2.00	197.4
GS-16	12	25	50	30	15	1.5	2.25	108.3
GS-17	12	25	50	30	10	1.5	4.00	8.2
GS-18	12	25	50	30	10	1.5	3.00	8.0
GS-19	12	25	50	30	10	1.5	2.50	6.8
GS-20	12	25	50	30	10	1.5	2.00	3.3
GS-21	12	25	50	30	10	1.5	2.25	4.9
GS-22	12	25	50	30	15	2.0	4.00	8.1
GS-23	12	25	50	30	15	2.0	3.00	6.7
GS-24	12	25	50	30	15	2.0	2.50	3.1
GS-25	12	25	50	30	15	2.0	2.00	94.3
GS-26	12	25	50	30	15	2.0	2.25	12.9

References

Al-Kindi, S., White, N., Sinha, M., England, R., and Tiley, R., 2003, Crustal trace of a hot convective sheet: Geology, v. 31, p. 207–210, doi: 10.1130/0091-7613(2003)031<0207:CTOAHC>2.0.CO;2

Bluck, B.J., Dempster, T.J., Aftalion, M., Haughton, P.D.W., and Rogers, G., 2006, Geochronology of a granitoid boulder from the Corsewall Formation (Southern Uplands): implications for the evolution of southern Scotland': Scottish Journal of Geology, v. 42, p. 29–35, doi: 10.1144/sjg42010029.

Braun, J., Van Der Beek, P., Valla, P., Robert, X., Herman, F., Glotzbach, C., Pedersen, V., Perry, C., Simon-Labric, T., and Prigent, C., 2012, Quantifying rates of landscape evolution and tectonic processes by thermochronology and numerical modeling of crustal heat transport using PECUBE: Tectonophysics, v. 524-525, p. 1–28, doi: 10.1016/j.tecto.2011.12.035.

Brown, P.E., Soper, N.J., and Miller, J.A., 1964, Age of the principal intrusions of the Lake District, *in* Proceedings of the Yorkshire Geological and Polytechnic Society, v. 34, p. 331–342, doi: 10.1144/pygs.34.3.331.

Brown, P.E., Miller, J.A., and Grasty, R.L., 1968, Isotopic ages of late Caledonian granitic intrusions in the British Isles, *in* Proceedings of the Yorkshire Geological and Polytechnic Society, v. 36, p. 251–276, doi: 10.1144/pygs.36.3.251.

Croudace, I.W., 1982, The geochemistry and petrogenesis of the Lower Paleozoic granitoids of the Lleyn Peninsula, North Wales: Geochimica et Cosmochimica Acta, v. 46, p. 609–621, doi: 10.1016/0016-7037(82)90162-4.

Donelick, R.A., Ketcham, R.A., and Carlson, W., 1999, Variability of apatite fission-track annealing kinetics: II. Crystallographic orientation effects: American Mineralogist, v. 84, p. 1224–1234, doi: 10.2138/am-1999-0902.

Downing, R.A., and Gray, D.A., 1986, Geothermal Energy: The potential in the United Kingdom: British Geological Survey, p. 187.

Dunkl, I., 2002, TRACKKEY: a Windows program for calculation and graphical presentation of fission track data: Computers & Geosciences, v. 28, p. 3–12, doi: 10.1016/S0098-3004(01)00024-3.

Eppelbaum, L., Kutasov, I., and Pilchin, A., 2014, Applied Geothermics: Springer, p. 751, doi: 10.1007/978-3-642-34023-9.

Gallagher, K., 2012, Transdimensional inverse thermal history modeling for quantitative thermochronology: Journal of Geophysical Research, v. 117, p. 1–16, doi: 10.1029/2011JB008825.

Halliday, A.N., Aftalion, M., van Breemen, O., and Jocelyn, J., 1979, Petrogenetic significance of Rb- Sr and U-Pb isotopic systems in the 400 Ma old British Isles granitoids and their hosts: Geological Society, London, Special Publications, v. 8, p. 653–661, doi: 10.1144/GSL.SP.1979.008.01.79.

Hurford, A.J., and Green, P.F., 1982, A users' guide to fission track dating calibration: Earth and Planetary Science Letters, v. 59, p. 343–354, doi: 10.1016/0012-821X(82)90136-4.

Ketcham, R.A., Carter, A.C., Donelick, R.A., Barbarand, J., and Hurford, A.J., 2007, Improved measurement of fission-track annealing in apatite using c-axis projection: American Mineralogist, v. 92, p. 789–798, doi: 10.2138/am.2007.2280.

Lee, M. K., Brown, G. C., Webb, P. C., Wheildon, J., and Rollin, K. E., 1987, Heat flow, heat production and thermo-tectonic setting in mainland UK: Journal of the Geological Society, v. 144, p. 35–42, doi: 10.1144/gsjgs.144.1.0035.

Manning, D. A. C., Younger, P. L., Smith, F. W., Jones, J. M., Dufton, D. J., Diskin, S., 2007, A deep geothermal exploration well at Eastgate, Weardale, UK: a novel exploration concept for low-enthalpy resources: Journal of the Geological Society, v. 164, p. 371–382, doi: 10.1144/0016-76492006-015.

Molnar, P., and England, P., 1990, Late Cenozoic uplift of mountain ranges and global climate change: chicken and egg?: Nature, v. 346, p. 29–34, doi: 10.1038/346029a0.

Rundle, C. C., 1979, Ordovician intrusions in the English Lake District: Journal of the Geological Society, v. 136, p. 29–38, doi: 10.1144/gsjgs.136.1.0029.

Stephenson, D., Loughlin, S.C., Millward, D., Waters, C.N., and Williamson, I.T., 2003 Carboniferous and Permian Igneous Rocks of Great Britain North of the Variscan Front: Geological Conservation Review Series, No. 27, Joint Nature Conservation Committee, Peterborough, 374 p.